Optical, thermal, and electrical monitoring of radio-frequency tissue modification

Timmy Floume
Imperial College London
Department of Electrical and Electronic Engineering
Exhibition Road
London SW7 2AZ, United Kingdom
and
Imperial College London
St Mary's Hospital
Department of Bio Surgery and Surgical Technology
Praed Street
London W2 1NY, United Kingdom

Richard R. A. Syms
Imperial College London
Department of Electrical and Electronic Engineering
Exhibition Road
London SW7 2AZ, United Kingdom

Ara W. Darzi
George B. Hanna
Imperial College London
St Mary's Hospital
Department of Bio Surgery and Surgical Technology
Praed Street
London W2 1NY, United Kingdom

Abstract. Radio-frequency (rf) tissue fusion involves the sealing of tissue between two electrodes delivering rf currents. Applications include small bowel fusion following anastomosis. The mechanism of adhesion is poorly understood, but one hypothesis is that rf modification is correlated to thermal damage and dehydration. A multimodal monitoring system capable of acquiring tissue temperature, electrical impedance, and optical transmittance at 1325-nm wavelength during rf delivery by a modified Ligasure™ fusion tool is presented. Measurements carried out on single layers of *ex vivo* porcine small bowel tissue heated at ≈500-kHz frequency are correlated with observation of water evaporation and histological studies on full seals. It is shown that the induced current generates a rapid quasilinear rise of temperature until the boiling point of water, that changes in tissue transmittance occur before impedance control is possible, and that a decrease in transmission occurs at typical denaturation temperatures. Experimental results are compared with a biophysical model for tissue temperature and a rate equation model for thermal damage. [DOI: 10.1117/1.3323089]

Keywords: radio-frequency tissue fusion; monitoring; tissue modification.

Paper 09139RR received Apr. 14, 2009; revised manuscript received Nov. 18, 2009; accepted for publication Jan. 4, 2010; published online Feb. 24, 2010.

1 Introduction

The process of radio-frequency (rf) tissue fusion involves clamping the tissue between two electrodes while holding opposing tissue faces under pressure.[1] A controlled RF voltage is then applied so that the rf current generates heat via the Joule effect, and tissue transformations such as denaturation and dehydration are induced by combined heat and pressure. The technology is now commonly used for hemostatic sealing of blood vessel and arteries, and research is being carried out to transfer it to other tissue types (e.g., small bowel) during other surgical procedures (e.g., bowel anastomosis).[1,2]

Energy delivery or dosimetry of energy-based therapy or surgical procedure has always been challenging, and tissue variability is a key difficulty. Significant improvement will follow from a better understanding of the tissue modifications that occur, not only allowing the development of effective energy delivery strategies but also enabling real-time feedback control.

Commercial equipment [such as the LigaSure™ (Valleylab, Boulder, Colorado), BiClamp™ (ERBE, Tubingen, Germany), and Seal™ (Gyrus PK, Wokingham, United Kingdom)] often makes use of the change in tissue electrical impedance to control rf delivery so that a reliable and reproducible seal is generated. However, a first important question is whether impedance-based feedback control suffers from any intrinsic limitations, since significant impedance changes might be expected to occur only in the final stage of rf delivery when tissue water boils. Optical measurements have been proposed as a method of monitoring tissue coagulation during thermotherapy such as rf ablation[3,4] or laser interstitial heating.[5,6] A second important question is therefore whether optical monitoring could be used to complement any deficiencies in impedance monitoring. We have already described one application of optical transmission spectroscopy in monitoring changes in tissue optical properties.[7] Here, we monitored dynamic changes in a broad spectrum surrounding a strong water absorption band at 1450-nm wavelength, focusing on differences between the absorption peak and the attenuation baseline to extract the attenuation and hence the water content. A third important question is whether changes in transmittance outside the absorption band could also be used as an indicator of thermal damage.

We attempt to answer these three questions using a system capable of simultaneously measuring tissue impedance, near-infrared optical transmittance, and temperature during rf modification of single layers of *ex vivo* bowel tissue. We compare temperature measurements with a simple biophysical model and transmittance measurements with a first-order Arrhenius rate-process model widely used to describe thermal damage in tissue,[8–12] and attempt direct correlations with histological examination of fused seals. We do not attempt to use the system for optimizing seal quality in a rf fusion process, although this is clearly an important future goal. In Sec. 2, we

Address all correspondence to: Timmy Floume, Imperial College London, Electrical and Electronic Engineering, Optical and Semi Conductor Group, Exhibition Road, London, SW7 2BT, United Kingdom. Tel: 44-207-59-46-216; Fax: 44-207-59-46-308; E-mail: t.floume@imperial.ac.uk

1083-3668/2010/15(1)/018003/10/$25.00 © 2010 SPIE

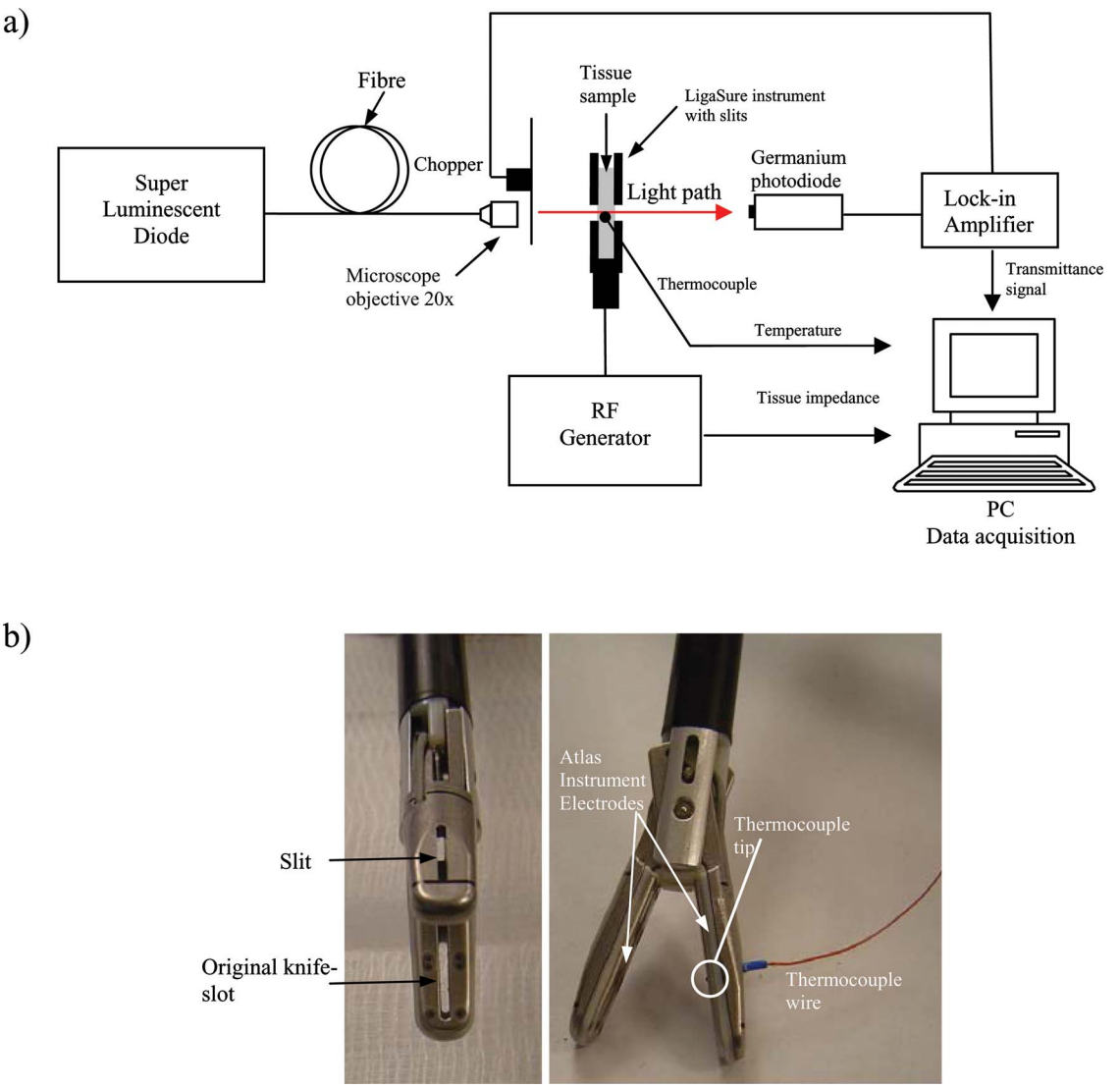

Fig. 1 (a) Experimental arrangement for simultaneous measurement of tissue transmittance and temperature. Light from a fiber-coupled superluminescent diode (1325 nm) is collimated and chopped before being passed in the tissue held between the jaws of the modified Atlas instrument shown in (b). Transmitted light is detected by a Germanium detector, and lock-in detection is used to improve signal-to-noise ratio. Tissue temperature and impedance are recorded simultaneously on a PC. (b) Modified Atlas LigaSure™ instrument (Valleylab, Tyco Healthcare) with slits on both jaws at the location of the knife slot and thermocouple. Note the position of the thermocouple, just above the electrode surface.

describe the experimental arrangement used to heat tissue using rf energy, and simultaneously measure temperature, electrical impedance, and optical transmission, calibration to known standards, a model for electrical heating, and a rate-process model for transmission changes. The results of experiments on *ex vivo* porcine small bowel tissue are presented and compared with theory in Sec. 3 and discussed further in Sec. 4. Conclusions are presented in Sec. 5.

2 Material and Methods

2.1 *Experimental Apparatus*

Figure 1(a) shows the complete experimental arrangement, which consists of an rf generator and heating electrodes, an impedance measurement system, a temperature measurement system, and a near-infrared transmission spectroscopy system.

2.1.1 *Radio-frequency delivery, impedance readout, and calibration*

The rf generator is a prototype developed by Valleylab (Boulder, Colorado)[1] capable of delivering a constant sinusoidal voltage (10, 15, and 20 V) and operating at 487 kHz. At this frequency, neuromuscular stimulation and electrocution are avoided. A blood vessel sealing tool, the LigaSure™ Atlas (Valleylab, Boulder, Colorado), was connected to the generator and used to apply pressure and rf heating to tissue clamped between its jaws, as shown in Fig. 1(b). To allow light transmission, 0.8-mm-wide slits were cut in both jaws at the location of the integrated knife slot normally used to divide blood vessels after sealing. Since the slot is narrow, this modification only affects the nontissue contacting parts of the jaw and not the electrode geometry. A compression spring in the handle guarantees constant pressure. The tissue within which

light propagates and temperature is measured is only pressurized at the edges.

The rf generator continuously monitors both the rms voltage and the current delivery to the instrument. The electrical impedance is then simply obtained by dividing the voltage readout by the current readout. Such processing enables the extraction of the "effective" tissue impedance only. Therefore, the measured impedance is the modulus of the potentially complex impedance of the instrument/tissue system, and the term "tissue impedance" is used to describe this quantity throughout. The electrical readout was calibrated using a set of high power resistors (50, 100, 200, and 400 Ω) and software linear correction. Good overall linearity was obtained.

2.1.2 *Temperature measurement and observation of tissue water vaporization*

Tissue temperature was measured using a fine (0.005-in.) wire Teflon-insulated J-type thermocouple (5TC-TT-J-36-36, Omega Engineering, Bridgeport, New Jersey), which was inserted through one of the slits and glued in place at the top of the slit so that its tip emerged 0.25 mm above the electrode surface. In this way the thermocouple is in contact with the tissue surface without piercing it, and is insulated from the electrode. The use of an electrical sensor in a high rf field is controversial. A strict calibration of temperature readout was therefore carried out using saline solution and cellulose phantoms. The use of a thermocouple was further validated by comparing its reading to results obtained with a thermal camera (FLIR Thermovision A40, Infrared System, Reno, Nevada). Similar results were obtained with the two modalities, suggesting that the thermocouple can be used without interference from rf currents. Similar heating patterns were observed with and without the thermocouple. Because the use of a thermal camera is cumbersome, subsequent measurements were carried out with the thermocouple alone.

To discuss the evolution of measurements during rf fusion, it is essential to consider the onset of tissue water evaporation. A simple arrangement was therefore used to investigate the timing of evaporation. A clean microscope slide was held just above the instrument to condense escaping steam, and the time between the start of rf delivery and the moment at which condensation is first observed was measured.

2.1.3 *Transmittance measurement*

Near-infrared tissue transmittance changes were measured at 1325-nm wavelength. This wavelength is outside the strong absorption band of water in tissue at 1460 nm, and this transmittance can be seen as the attenuation baseline of the transmission spectra in Ref. 7. The light source was a fiber-coupled superluminescent diode (Superlum, Moscow, Russia) with a bandwidth of 50 nm. Light from the diode was coupled via a single-mode optical fiber to a 20× microscope objective, which formed a quasicollimated Gaussian beam of ≈0.7-mm mode field diameter.

The light beam was passed through the tissue held between the electrodes of the modified Atlas™ instrument to a detector [Fig. 1(a)]. To improve dynamic range, the detection apparatus used is different from that in Ref. 7, where transmitted light was coupled into an optical fiber via a microscope objective. Instead, a 1-mm-diam germanium photodetector, based on a commercial photodiode with a response to 1.6-μm wavelength and a custom transimpedance amplifier, was used. The detector was placed 10 cm behind the tissue, resulting in a detection angle of 10 mrad. This angle guarantees that a negligible amount of diffusely transmitted light is detected and consequently the measured signal is proportional to the collimated transmitted light.

Noise was minimized by chopping the light beam before it entered the tissue and measuring the photodiode signal with a lock-in amplifier (Princeton Applied Research, model 5209, Oak Ridge, Tennessee). Temperature, impedance, and the transmittance signal from the lock-in amplifier were acquired synchronously at 100 Hz by a data acquisition system (DAQpad 5062e, National Instruments, Austin, Texas), connected to a standard personal computer via a Labview (National Instruments) interface.

2.1.4 *Tissue preparation, statistical analysis, and histology*

Samples of porcine small bowel tissue (15 cm long) were obtained from a slaughterhouse washed and frozen at -17 °C. Samples frozen for no more than 4 weeks were used. Samples were thawed at room temperature and washed again to eliminate any remaining luminal content. The bowel samples were then dissected along the connection to the mesentery. Prepared bowel samples were kept hydrated between humidified gauze before use. A single thickness of the porcine small bowel wall was held between the jaws of the modified vessel sealing instrument.

Because tissue is intrinsically variable, it is hard to obtain truly reproducible results. A statistical analysis was therefore carried out on 20 repeat experiments to obtain significant information on the correlations between the different measurement evolutions. Whenever possible, the times between simultaneous measurements made on a single sample were compared, as it reduced in part the sample-to-sample variability, and also because when feedback control is envisaged, it is the correlation in each sample that matters. To determine the degree of temporal correlation between physical processes, both the average and standard deviations of the time difference between pairs of events were determined.

To assess the structural changes inflicted to the tissue qualitatively, histological examination of rf-fused tissue was carried out. Samples of porcine small bowel were fused and histological sections were taken before and after fusion. The samples were dissected and conserved in formaldehyde, stained with hematoxylin and eosin, and slices transversal to the seal were prepared on microscope slides.

2.2 *Theoretical Models*

Two simple models were developed to understand the consequence of rf heating: a biophysical model of temperature evolution, and a rate equation model of damage.

2.2.1 *Biophysical model of tissue temperature*

To describe the initial phase of tissue heating, we use a simplified lumped thermodynamical model accounting for heat exchange between the tissue and the surrounding instrument. We assumed that heat is deposited in the tissue by rf current dissipation and lost only by solid conduction with the instru-

ment electrode. We neglected the effect of heat convection inside the tissue and at the tissue-air interface, although in a surgical setting with *in vivo* tissue, the presence of blood flow will almost certainly further increase heat loss. We also assumed that the tissue temperature is uniform and that the instrument temperature stays constant at room temperature (T_r) for the duration of the experiment (i.e., that the tissue is heated more rapidly than the instrument itself). The variation of thermal energy of the tissue per unit volume is then given by:

$$\rho C_T \frac{\partial T}{\partial t} = \frac{U^2}{R_{\text{elec}} V} - \frac{\sigma S}{V}[T(t) - T_r], \tag{1}$$

where ρ and C_T are the tissue density and specific heat capacity. U is the applied voltage, and R_{elec} and V are the electrical resistance and volume of the tissue, respectively. The first term on the right-hand side of Eq. (1) is the power generated in the tissue per unit volume due to rf dissipation. The second term in Eq. (1) accounts for heat exchange between the tissue at temperature T and the instrument at temperature T_r. σ is the overall thermal conduction coefficient $[W.^{\circ}C^{-1}.M^{-2}]$ at the tissue/instrument interface of surface S $[M^2]$, which is a function of its thermal conduction properties.

By solving Eq. (1), one obtains the following expression for the temperature elevation:

$$T(t) = T_r + \frac{((U^2/R_{\text{elec}}V) + (\sigma S/V)T_r)}{\sigma S/V}\left[1 - \exp\left(-\frac{\sigma S}{V\rho C_T}t\right)\right]. \tag{2}$$

Assuming now that the term $\sigma St/V\rho C_T$ is small (i.e., that the interface between tissue and electrodes is quasiadiabatic), this result can be approximated as:

$$T(t) = T_r + \frac{1}{\rho C_T}\left(\frac{U^2}{R_{\text{elec}}V} + \frac{\sigma S}{V}T_r\right)t. \tag{3}$$

The rate of temperature rise R_T as a function of the applied voltage and the electrical and thermal characteristic of the tissue is then given by:

$$R_T = \frac{1}{\rho C_T}\left(\frac{U^2}{R_{\text{elec}}V} + \frac{\sigma S}{V}T_r\right). \tag{4}$$

R_T therefore varies linearly with U^2, a feature that should be experimentally verifiable.

2.2.2 *Rate equation model of tissue damage*

Previous studies where changes in the optical properties of tissue are compared with a rate-process model generally involve heating the tissue at a constant temperature and measuring changes after or during heating.[11–13] An implicit assumption is often that the rate constant is fixed, and the effect of the rise from room temperature to the operating temperature is ignored when fitting the experimental data. If important modifications of measured properties occur during this phase, the temperature dependence of the rate constant must be taken into account. Henriques[9] was first to propose an Arrhenius formulation for a dimensionless degree of damage Ω as:

$$\Omega(\tau) = -\ln\left[\frac{c(\tau)}{c(0)}\right] = \int_0^\tau k(t)dt = \int_0^\tau A\exp[-E_a/RT(t)]dt, \tag{5}$$

where $c(\tau)$ represents the concentration of undamaged tissue at time τ and $c(0)$ is the initial concentration. $k(t)$ is the rate constant of the transformation at time t. A is the frequency factor (s^{-1}) and E_a (J) is the activation energy. R is the gas constant and $T(t)$ is the temperature in degrees Kelvin. A and E_a can be expressed in terms of molar entropy ΔS ($J\,mol^{-1}\,K^{-1}$), and molar enthalpy ΔH ($J\,mol^{-1}$) of the reaction[13] as:

$$E_a = \Delta H,$$

$$A = \frac{k_B T}{h}\exp(\Delta S/R), \tag{6}$$

where k_B is Boltzmann's constant (1.381×10^{-23} J K^{-1}) and h is Planck's constant (6.626×10^{-34} J s). The degree of damage can then be rewritten as:

$$\Omega(\tau) = -\ln\left(\frac{c(\tau)}{c(0)}\right) = \int_0^\tau \frac{k_b T(t)}{h}\exp(\Delta S/R)\exp[-E_a/RT(t)]dt. \tag{7}$$

In this form, the influence of temperature is fully accounted for. The damage fraction f_d, defined as the ratio of the concentration of damaged tissue to the initial concentration, can be written as:[14]

$$f_d(t) = \frac{c(0) - c(t)}{c(0)} = 1 - \exp[-\Omega(t)]. \tag{8}$$

Thus f_d varies from 0 when there is no tissue damage, to 1 for complete damage.

This model can be related to transmittance measurement as follows. The intensity of detected light $I(t)$ is given by the Beer-Lambert law:

$$I(t) = I_0\exp\{-[\mu_s(t) + \mu_a(t)]d\}. \tag{9}$$

Here I_0 is the light intensity incident on the tissue, $\mu_s(t)$ and $\mu_a(t)$ are the scattering and absorption coefficient of the tissue at time t, and d is the optical path length in the tissue. Numerous studies have shown that thermal damage mainly results in an increase of the scattering coefficient of the tissue, and that scattering is more important than absorption.[12,15] Assuming that changes in transmittance are mainly due to changes in scattering, the following model can be used to describe the changes in scattering coefficient:

$$\begin{aligned}\mu_s(t) &= \mu_s(0)\{1 - f_d(t)\} + \{\mu_s(0) + \Delta\mu_s\}f_d(t)\\ &= \mu_s(0) + \Delta\mu_s f_d(t).\end{aligned} \tag{10}$$

Here $\mu_s(0)$ is the undamaged tissue scattering coefficient and $\Delta\mu_s$ is the increase of scattering coefficient due to heating. Defining the normalized transmittance T_{norm} as the ratio

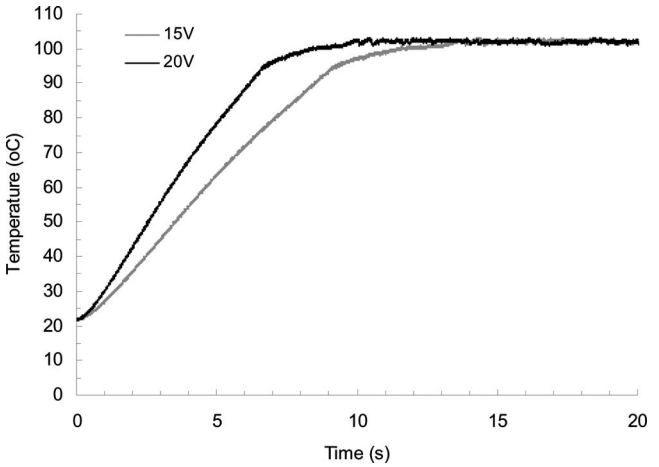

Fig. 2 Temperature measurements during rf application with the instrument immersed in saline.

of the intensity detected at time t to the intensity before rf application, and using Eq. (10) to express the changes in scattering, T_{norm} can be expressed as:

$$T_{\text{norm}}(t) = \exp[-f_d(t)\Delta\mu_s d]. \quad (11)$$

This result provides a clear connection between the damage fraction and the optical transmittance, and was used to fit experimental data. Matlab (Natick, Massachusetts) was used to determine $f_d(t)$ numerically, based on the experimental recording of the temperature evolution and assumed values of ΔS and ΔH. Unfortunately, the experimental setup did not have sufficient dynamic range to allow measurement of the normalized transmission when f_d approached 1, which would have enabled calculation of $\Delta\mu_s d$ directly. To overcome this limitation, measurement of the time $t_{36\%}$ at which T_{norm} reached 36% of its initial value was used. $f_d(t_{36\%})$ was then calculated using the fitting parameters ΔS and ΔH. Equation (11) was then used to fit measured data, in the modified form:

$$T_{\text{norm}}(t) = \exp\{-f_d(t)/f_d(t_{36\%})\}. \quad (12)$$

This result allows matching to experimental measurements of T_{norm} based on the two constants ΔS and ΔH only.

3 Results

3.1 *Temperature Evolution in Saline and Cellulose Phantoms*

Figure 2 shows typical temperature measurements obtained during rf deposition in saline. The temperature evolution typically consists of a quasilinear increase until the boiling point is reached. However, the temperature sometimes rose above 100 °C for a short period, presumably because of superheating. Similar experiments carried out on wet cellulose (surgical-grade paper), to investigate if the presence of a solid body between the jaws of the instrument and contacting the thermocouple affects the measurement, showed more variability. However, the temperature evolution was similar, with a rapid quasilinear increase until boiling, at which point steam escape was observed. Results obtained from 20 samples are summarized in the first rows of Table 1 in terms of rate of temperature rise. No change in temperature was observed when rf power was applied with the jaws of the instrument held open.

3.2 *Temperature Evolution in Bowel Tissue*

Figure 3 shows typical measurements of normalized transmission, impedance, and temperature as a function of time during rf heating for three bowel tissue samples. The temperature

Table 1 Summary of timing measurements on phantoms and tissue. Δ is the time between tissue reaching 100 °C, and the start of impedance rise Δ′ is the time between observation of stream escape and the start of impedance rise.

Sample	Voltage (V)	Number of samples	Average of temperature rise (°C s^{-1})	Average duration Δ	Standard deviation of Δ	Average duration Δ′	Standard deviation of Δ′
Saline	10	20	0	X	X	X	X
"	15	20	8.1	X	X	X	X
"	20	20	11.31	X	X	X	X
Cellulose +saline	10	20	9.35	X	X	X	X
"	15	20	11.3	X	X	X	X
"	20	20	14.8	X	X	X	X
Bowel tissue	10	20	8.8	X	X	X	X
"	15	20	10.2	6.8	1.9	3.9	1.8
"	20	20	14.1	5.2	1.05	3.1	1.6

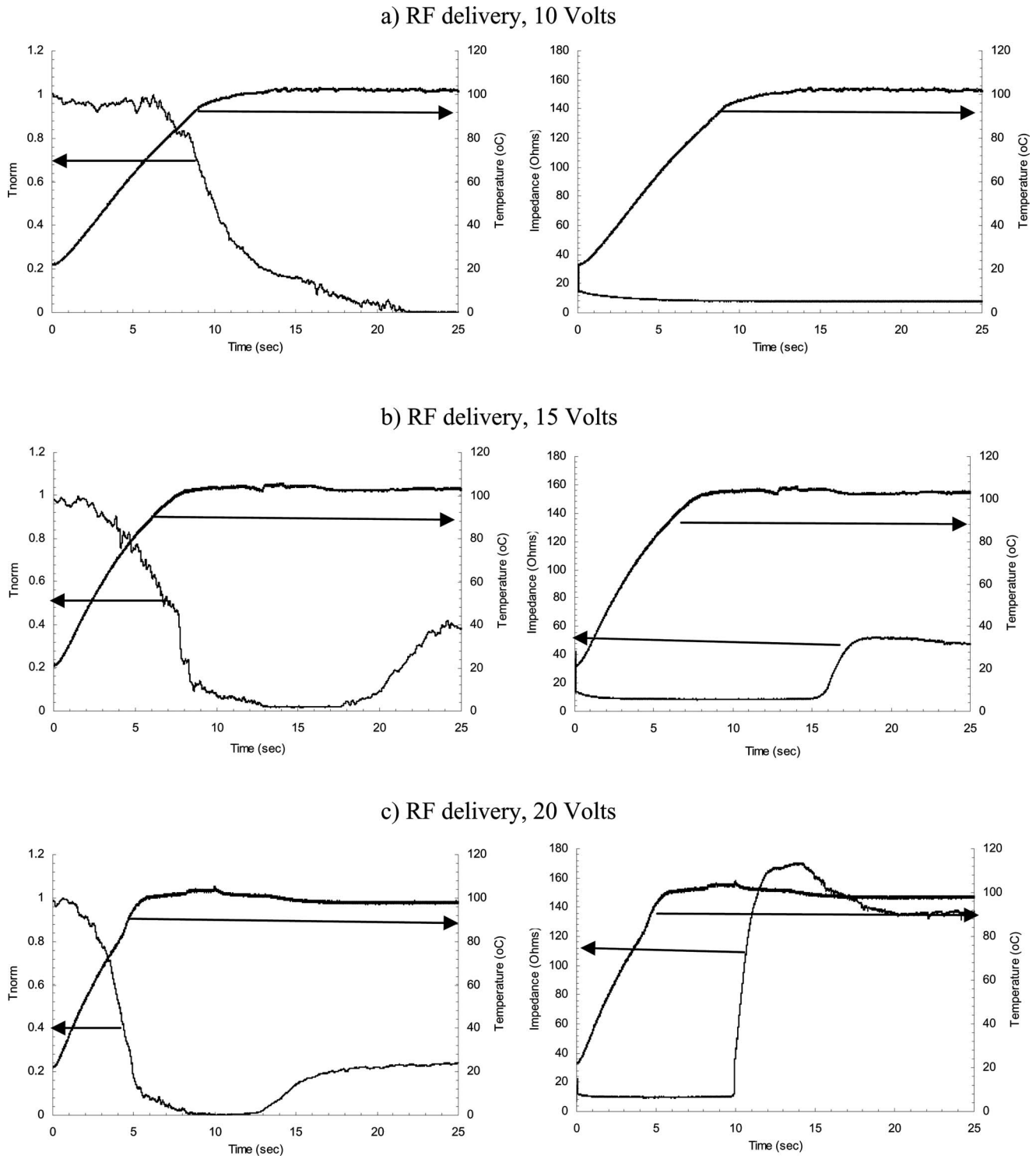

Fig. 3 Simultaneous measurements of tissue normalized transmittance (T_{norm}), temperature, and impedance during rf heating at three different rf voltages of (a) 10, (b) 15, and (c) 20 volts. Left column: normalized transmittance (left axis) and tissue temperature (right axis) against time in seconds. Right column: Tissue impedance (left axis) and temperature (right axis) against time in seconds.

evolution again consists of a quasilinear increase from room temperature (20 °C) to approximately 100 °C for all three voltages considered. After reaching 100 °C, the temperature stays constant. In this stage, phase transfer consumes most of the rf energy delivered to the tissue.

The rate of the initial temperature rise increases with the applied rf voltage. Linear regression performed during the initial phase (below 100 °C) for 20 tissue samples at each voltage gives an average rate of temperature increase of 8.8 °C s^{-1}, 10.8 °C s^{-1}, and 14.1 °C s^{-1} for 10, 15, and

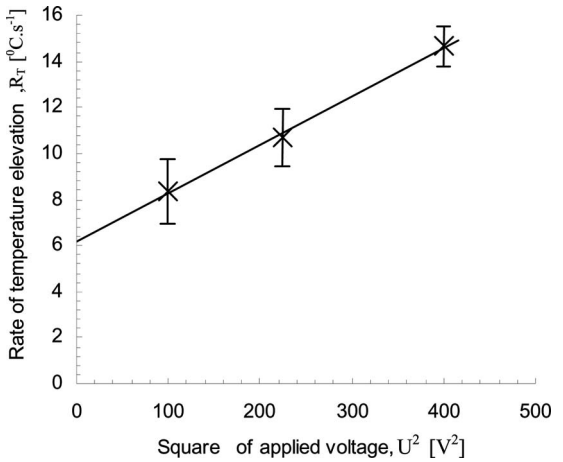

Fig. 4 Experimental values of rate of temperature rise against the square of the applied voltage.

20 V, respectively. Figure 4 shows the variation of these values with the square of the applied voltage. The linearity assumed by Eq. (4) is clearly verified. Linear regression gives a y-intercept of 6.1. This suggests that $\sigma S T_r / V \rho C_T \approx 6.1$ K. s^{-1}, which in turn shows that the assumption made in Eq. (3) ($\sigma S t / V \rho C_T \ll 1$) is valid for a time $t \ll T_r / 6.1$. For a 293 K room temperature, this translates into $t \ll 47$ s, which is again verified experimentally, as the temperature rise took place in less than 10 s. These conclusions validate the assumptions of the model.

3.3 *Impedance Evolution in Bowel Tissue*

Figure 3 also shows the typical evolution of tissue temperature and impedance during rf delivery. The final rise of impedance is a strong function of the applied voltage. At low voltage (10 V), significant changes are not observed. The impedance decreases slightly as the temperature rises, and then stays constant at a low value of about 10 Ω. For higher applied voltages (15 and 20 V), the impedance evolution is different. At both voltages, the impedance initially decreases slightly (as at lower voltage) and then dramatically increases (after about 16 and 10 s, at 15 and 20 V, respectively). In the 20 repeated experiments, it was found that the increase of impedance always follows the leveling of the temperature at 100 °C. Furthermore, the faster the tissue reaches the boiling point, the faster the impedance increase occurs. The rate of increase and final level of impedance is also generally a function of the applied voltage: the higher the voltage, the faster and larger the impedance rise.

The results of all experiments are again summarized in Table 1. For all voltages, the average time between the points at which impedance starts to rise and the temperature reaches 100 °C (defined as Δ) is 6 s, with a standard deviation of 1.5 s. Since the standard deviation is small compared to Δ, there must be a strong causality between tissue water boiling and impedance rising. These results are compared with the time between the points at which the impedance rise starts and steam is observed (defined as Δ′). There is again a strong correlation, confirming that impedance changes are due to a reduction in water content following boiling.

In fact, we believe that the rapid increase of impedance is the combined result of water loss due to evaporation, and the formation of steam vacuoles in the tissue and at the tissue/electrode interface, which results in the formation of nonconductive domains. The first phenomenon explains why the impedance rise always closely follows the tissue reaching the boiling point of water. The second could explain the fact that the overall impedance change is more significant at a higher voltage when more thermal energy is delivered into the tissue and the rate of steam generation may be more important. The reason that changes in impedance are not observed at 10 V could be that at this voltage, the rate of steam generation is insufficient to drive water away from the seal. In fact no steam escape was observed during such experiments.

3.4 *Transmittance Evolution in Bowel Tissue*

The left column of Fig. 3 also shows the evolution of tissue temperature and normalized transmittance during rf delivery at the three voltages. The transmitted intensity starts to decrease dramatically during the phase of temperature rise. The faster the temperature increases, the faster the transmittance decreases. Explanation may be provided by consideration of thermal damage. Damage results from several tissue transformations, including protein denaturation and coagulation, and modification of the tissue microstructure, such as shrinkage of collagen fiber[16] and deformation of mitochondria.[17] It generally occurs at temperatures above 60 °C. When the temperature rise is slow (10 V rf), the decrease of transmittance continues when the boiling temperature is reached, whereas for faster temperature rises (15 and 20 V), the decrease is quasi-complete when the temperature reaches 100 °C.

An increase of transmittance can also be seen in Figs. 3(b) and 3(c) after 18 and 12.5 s, respectively. This increase occurs after the temperature reaches 100 °C, and in each case follows closely the rapid impedance rises at 16 and 10 s, respectively. This increase in transmittance may be attributed to dehydration. As water is the principal absorber at the wavelength considered, a decrease of water content due to evaporation must reduce the absorption coefficient, resulting in an increase of transmittance. Lin, Motamedi, and Welch[18] also suggested that dehydration may enhance the forward scattering of the cell, which may cause an increase of the total transmission. Tissue shrinkage may also result in an increase in transmittance, since it decreases the optical path. However, no noticeable shrinkage was observed during our experiments. It has also been suggested that denser packing of cells can be induced by dehydration, and results in a decrease of the refractive index mismatch in the tissue and therefore a reduction of its scattering properties.

3.5 *Comparison with Thermal Damage Model*

Figure 5 shows measurements of normalized transmittance from the three samples of Fig. 3 and fitted curves calculated using the rate process model in Sec. 2.2. The temperature evolutions measured at each voltage were used to calculate the variation of the damage fraction with time. ΔS and ΔH were iteratively changed to maximize the agreement between fitted curves and experimental data, using values reported by Jacques[13] as a starting point.

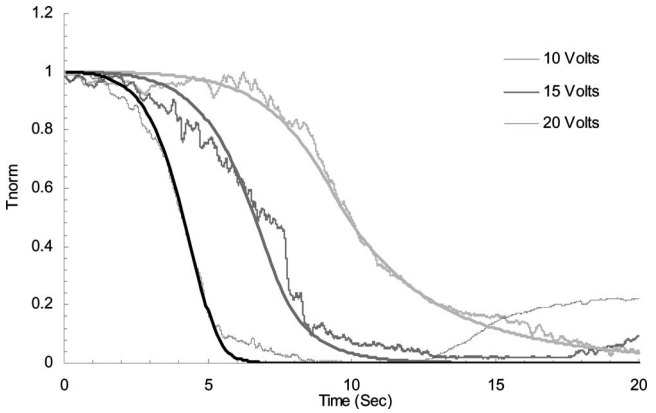

Fig. 5 Experimental and fitted curves of normalized transmittance during rf delivery at different constant voltage, as indicated in the legend.

Figure 5 compares the prediction of the rate-process model and the experimental data using the rate coefficients ($\Delta S = -82.9$ J mol^{-1} K^{-1} and $\Delta H = 7.18 \times 10^4$ J mol^{-1}) determined experimentally by Skinner et al.[12] for the changes in the reduced scattering coefficient of *ex vivo* rat prostate. All observed trends are predicted well. This qualitative agreement suggests that the changes in transmittance could be mainly due to an increase of the reduced scattering coefficient of the tissue, and that the thermal damage inflicted on porcine bowel during our experiments is similar to that observed in Skinner's study.

3.6 *Histological Studies*

Figure 6 shows histological results that demonstrate important changes in tissue structure arising during rf fusion. Figure 6(a) shows a section of porcine small bowel. The demarcation between structurally different bowel layers (i.e., mucosa, submucosa, and serosa) is clearly apparent. Figure 6(b) shows a section of an rf-induced seal. Comparison with Fig. 6(a) shows that fusion induces significant changes in the tissue structure. The delimitation between submucosa and mucosa is less clear, and the mucosa layer has reduced considerably in thickness. Finally, structurally noticeable features apparent in Fig. 6(a) have disappeared and are replaced by a more homogeneous coagulum.

Figures 6(c)–6(f) show views at 10× magnification of histological sections of tissue after undergoing rf heating at 20 V for 5, 10, 15, and 20 s, respectively. These results show that the mucosal layer seems to disintegrate during RF fusion. Its thickness [see mark M in Figs. 6(c) and 6(d)] first reduces, and the mucosal layer then seems to disappear or mix with the submucosal layer [white arrows in Figs. 6(e) and 6(f)]. Our thawed tissue sample does not enable a detailed histological examination. However, comparison of Figs. 6(c)–6(f) shows the gradual disappearance of structural features leading to the formation of a homogeneous amalgam of tissue residues.

4 Discussion

The motivation of this study was to investigate the evolution of and correlations between tissue temperature, impedance, and transmittance during rf heating, and their implications for the monitoring of tissue fusion. This enables us to investigate

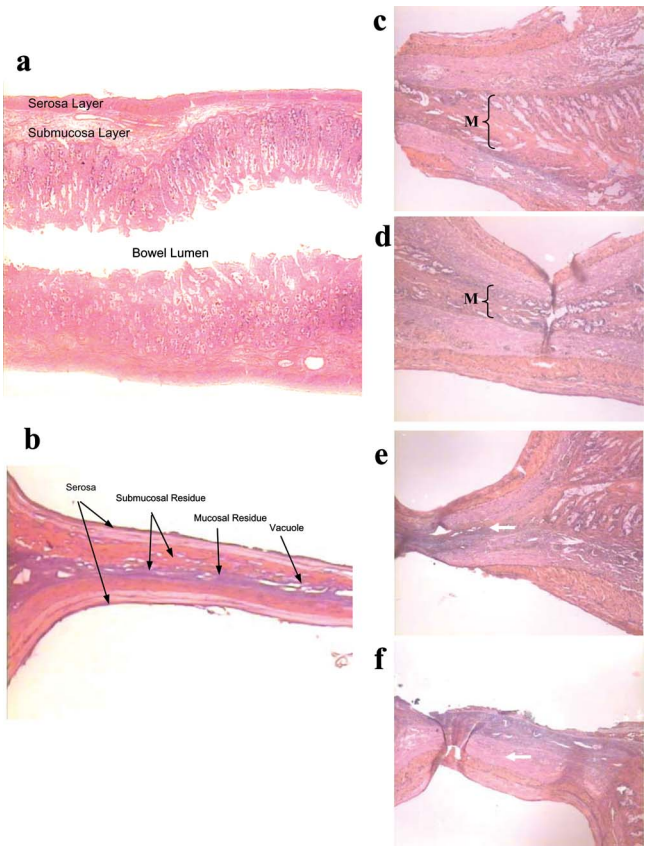

Fig. 6 Histological sections of fused and unfused porcine small bowel tissue: (a) unfused (2.5×) and (b) fused (10×). (c), (d), (e), and (f) show tissue fused at 20 V for 5, 10, 15, and 20 s, respectively. M on (c) and (d) indicates mucosal layers; white arrows on (e) and (f) show disappearance of mucosal layers.

further limitations of impedance feedback and to examine the significance of using optical measurement for the real-time assessment and control of thermal damage. The results of our experiments enable us to discuss the dynamics of the biophysical processes taking place during rf fusion. We now consider each of these points.

4.1 *Rate-Process Model of Transmittance Change*

Several authors have investigated the change in optical properties due to thermal damage. Derbyshire, Bogen, and Unger,[19] and Splinter et al.[20] studied thermally induced optical property changes of myocardium tissue. They demonstrate irreversible changes between 60 and 75 °C, the temperature range within which extracellular proteins and collagen denaturation are known to occur. They speculated that protein denaturation is responsible for the increase of scattering coefficient. Pickering et al.[21] pursued this study on myocardium and also showed that the reduced scattering coefficient of the tissue increases when heated. Bosman[22] used transmission electron microscopy to characterize the structural changes induced by heating of Pickering's samples. She showed that mitochondria fragments and myofilaments start to disintegrate into smaller granules as a result of heating. Thomsen, Jacques, and Flock[23] have described equivalent ultrastructural changes of thermally coagulated rat myocardium: disruption of mito-

chondria and formation of small aggregates resulting from the denaturation of fibrillar protein and other cytoplasmic constituents.

Direct correlation between tissue transmittance changes and microscopic thermal damage is challenging, mainly because histological examination is qualitative, and the microscopic origins of tissue optical properties are complex and multiple.[24] However, we believe that our results show that transmittance change is a good candidate as an indirect measurement of damage. First, as discussed before, it has been shown by many authors that thermal damage results in optical property changes and especially scattering increase. Second, we observed changes in transmittance starting at temperatures known to damage tissue (i.e., above 60 °C), but not at lower temperatures. Finally, as shown in Fig. 5, measured changes in transmittance can be modeled well by using a first-order rate process to describe the influence of thermal damage on scattering. Although this approach is generally used to describe damage under isothermal conditions, it can still be used to describe dynamic changes, as in our experiments. This result further demonstrates the versatility of the model.

We do, however, note that the method used is not one of choice for the precise determination of the thermodynamical parameters (ΔS, ΔH) involved. Traditional methods, consisting of heating the tissue at a constant temperature for different durations and measuring damage-related changes, are more precise, and enable the straightforward fitting of a large quantity of data obtained under known conditions by simpler expressions.[13] Therefore, the correlations between the model and our measurements principally demonstrate the applicability of modeling dynamic changes with a theoretical expression generally used to describe thermal damage.

4.2 *Dynamics of Tissue Transformations During Radio-Frequency Delivery*

We believe that the outcome of rf tissue fusion can be optimized by guaranteeing a better control of the induced tissue transformations, and that controlling denaturation and dehydration should lead to the formation of stronger and more reliable seals. The agreement between our model and experiments suggests that denaturation (observed as a decrease of tissue transmittance) can still occur when water evaporation starts (i.e., when evaporation occurs at 100 °C), especially if the initial heating rate is fast. Thus, a simple phenomenological model will consist of dividing the tissue transformation into three phases: the first when temperature increases and the tissue starts to denature, the second when water evaporates and denaturation is still in progress, and a possible third when quasitotal denaturation is achieved and the tissue continues to dehydrate.

Tissue transformations during rf application show that our model of thermal damage is likely to be incomplete, as it does not consider the interdependence between tissue denaturation and dehydration. For example, it is likely that the evaporation of water will generate damage of a different type than the mainly biochemical one described here. On the other hand, the denaturation of macromolecules and the thermal damage of tissue microstructure may modify its ability to desiccate through evaporation. For example, coagulation of macromolecules may generate more free water molecules, normally bound to protein, that evaporate more easily. The rupture of structural impermeable membrane, due to the mechanical strain induced by steam expansion, may also facilitate the evaporation of tissue water. It has been suggested that several rate processes, with several thermodynamical parameters, might be used.[14,16]

4.3 *Feedback Control of Radio-Frequency Delivery*

The results of Fig. 3 clearly demonstrate that the tissue impedance does not change significantly during the initial temperature rise. However, during this phase, denaturation is known to occur when the temperature exceeds about 60 °C. Therefore, the use of impedance as the sole feedback parameter to control RF delivery can only offer limited control in the initial phase. From Fig. 2 we see that tissue impedance change only occurs after the boiling point is reached, implying that impedance evolution is more likely to correlate with tissue water loss through evaporation. However, according to our own results (not presented here), tissue impedance at the end of fusion does not strongly correlate with its state of desiccation. As a result, we conclude that the impedance rise is most likely induced by the formation of nonconductive steam domains in the tissue and at the tissue/electrode interface. Other authors investigating RF tissue ablation have reached similar conclusions.[25]

In contrast to impedance, tissue transmittance changes dramatically during the initial temperature rise, which makes it a good candidate as a feedback parameter to control rf delivery during this phase. The good results of theoretical modeling of transmittance changes based on a first-order rate-process model further confirm that this approach can be used for monitoring. Protein (e.g., collagen) denaturation and crosslinking have been suggested as the leading mechanism of tissue fusion.[26,27] Therefore, assessing thermal damage in real time using transmittance changes even as an indirect measurement could prove very beneficial, both to investigate experimentally the role of denaturation in tissue fusion and ultimately to develop control algorithms based on transmittance measurements.

The main limitation of our experimental setup is the limited dynamic range of the optical detection system. We were unable to measure tissue transmittance precisely when the attenuation induced by thermal damage becomes too strong. Consequently, our model describes the initial phase of denaturation well, but our measurement does not enable us to verify its validity for more advanced damage. However, it is likely that transmittance will be affected by transformations other than the one described by our rate-process model. Water loss is likely to decrease optical absorption, and tissue damage induced by steam formation may further modify the scattering. Our model should therefore be improved by incorporating the contributions of those events.

5 Conclusions

We present the measurement of tissue temperature, impedance, and near-infrared transmittance during rf tissue fusion. Our results indicate that tissue impedance is largely insensitive to the initial tissue denaturation, whereas tissue transmittance is very sensitive. A first-order rate-process model is used to describe the changes in transmittance during the phase of

temperature elevation. The strong correlation with experiment suggests that a rate process can be used to model thermal damage under nonisothermal conditions, and that initial tissue transmittance changes can be used as indicators of thermal damage. Measurements of tissue temperature and impedance show that impedance changes only occur once the boiling point of water is reached. Therefore, the early stage of thermal damage cannot be controlled by using impedance as the sole feedback parameter. Optical monitoring is a promising alternative to impedance monitoring as a method for further understanding the dynamics of tissue modifications during rf fusion and for feedback control of rf delivery. This work should lead to the improvement of rf fusion and its transfer to other tissue types.

Acknowledgments

The authors are extremely grateful to Tyco Healthcare for financial support and to John Carlton of Valleylab for the provision of equipment and valuable technical assistance. The authors would particularly thank Robert Goldin of Saint Mary's Hospital, Imperial College, London, for the provision of histological samples.

References

1. C. A. Shields, D. A. Schechter, P. Tetzlaff, A. L. Baily, S. Dycus, and N. Cosgriff, "Method for creating ideal tissue fusion in soft-tissue structures using radio frequency (RF) energy," *Surg. Technol. Int.* **13**, 49–55 (2004).
2. J. F. Smulders, I. H. de Hingh, J. Stavast, and J. J. Jackimowicz, "Exploring new technologies to facilitate laparoscopic surgery: creating intestinal anastomoses without sutures or staples, using a radio-frequency-energy-driven bipolar fusion device," *Surg. Endosc* **21**(11), 2105–2109 (2007).
3. W.-C. Lin, C. Buttemere, and A. Mahadevan-Jansen, "Effect of thermal damage on the *in vitro* optical and fluorescence characteristics of liver tissue," *IEEE J. Sel. Top. Quantum Electron.* **9**(2), 162–170 (2003).
4. C. R. Buttemere, R. S. Chari, C. D. Anderson, M. K. Washington, A. Mahadevan-Jansen, and W. C. Lin, "*In vivo* assessment of thermal damage in the liver using optical spectroscopy," *J. Biomed. Opt.* **9**(5), 1018–1027 (2004).
5. A. Terenji, S. Willmann, J. Osterholz, P. Hering, and H. J. Schwarzmaier, "Measurement of the coagulation dynamics of bovine liver using the modified microscopic Beer-Lambert law," *Lasers Surg. Med.* **36**(5), 365–370 (2005).
6. J. P. Ritz, A. Roggan, C. T. Germer, C. Isbert, G. Muller, and H. J. Buhr, "Continuous changes in the optical properties of liver tissue during laser-induced interstitial thermotherapy," *Lasers Surg. Med.* **28**(4), 307–312 (2001).
7. T. Floume, R. R. A. Syms, A. W. Darzi, and G. B. Hanna, "Rea-time optical monitoring of radio frequency tissue fusion by continuous wave transmission spectroscopy," *J. Biomed. Opt.* **13**(6), 064006 (2008).
8. B. Chen, S. L. Thomsen, R. J. Thomas, J. Oliver, and A. J. Welch, "Histological and modeling study of skin thermal injury to 2.0 μm laser irradiation," *Lasers Surg. Med.* **40**(5), 358–370 (2008).
9. F. C. Henriques, "Studies of thermal injuries V: the predictability and the significance of thermally induced rate processes leading to irreversible thermal injury," *Am. J. Pathol.* **23**, 489–502 (1947).
10. R. Agah, A. H. Gandjbakhche, M. Motamedi, R. Nossal, and R. F. Bonner, "Dynamics of temperature dependent optical properties of tissue: dependence on thermally induced alteration," *IEEE Trans. Biomed. Eng.* **43**(8), 839–846 (1996).
11. R. Agah, J. A. Pearce, A. J. Welch, and M. Motamedi, "Rate-process model for arterial tissue thermal-damage—Implications on vessel photocoagulation," *Lasers Surg. Med.* **15**(2), 176–184 (1994).
12. M. G. Skinner, S. Everts, A. D. Reid, I. A. Vitkin, L. Lilge, and M. D. Sherar, "Changes in optical properties of *ex vivo* rat prostate due to heating," *Phys. Med. Biol.* **45**(5), p. 1375–1386 (2000).
13. S. L. Jacques, "Ratio of entropy to enthalpy in thermal transitions in biological tissues," *J. Biomed. Opt.* **11**(4), 041108 (2006).
14. J. A. Pearce and S. Thomsen, "Rate process analysis of thermal damage," in *Optical-Thermal Response of Laser-Irradiated Tissue*, A. J. Welch and M. J. C. van Gemert Eds, Plenum, New York, (1995).
15. J. P. Ritz, A. Roggan, C. Isbert, G. Muller, H. J. Buhr, and C. T. Germer, "Optical properties of native and coagulated porcine liver tissue between 400 and 2400 nm," *Lasers Surg. Med.* **29**(3), 205–212 (2001).
16. S. S. Chen, N. T. Wright, and J. D. Humphrey, "Phenomenological evolution equations for heat-induced shrinkage of a collagenous tissue," *Biomed. Eng.* **45**(10), 1234–1240 (1998).
17. G. Schuele, E. Vitkin, P. Huie, C. O'Connell-Rodwell, D. Palanker, and L. T. Perelman, "Optical spectroscopy noninvasively monitors response of organelles to cellular stress," *J. Biomed. Opt.* **10**(5), 051404 (2005).
18. W. C. Lin, M. Motamedi, A. J. Welch, "Dynamics of tissue optics during laser heating of turbid media," *Appl. Opt.* **35**(19), 3413–3420 (1996).
19. G. J. Derbyshire, D. K. Bogen, and M. Unger, "Thermally induced optical property changes in myocardium at 1.06 μm," *Lasers Surg. Med.* **10**(1), 28–34 (1990).
20. R. Splinter, R. H. Svenson, L. Littmann, J. R. Tuntelder, C. H. Chuang, G. P. Tatsis, and M. Thompson, "Optical properties of normal, diseased, and laser photocoagulated myocardium at the Nd:YAG wavelength," *Lasers Surg. Med.* **11**(2), 117–124 (1991).
21. J. W. Pickering, S. Bosman, P. Posthumus, P. Blokland, J. F. Beek, M. J. C. Vangemert, "Changes in the optical-properties (at 632.8 Nm) of slowly heated myocardium," *Appl. Opt.* **32**(4), 367–371 (1993).
22. S. Bosman, "Heat-induced structural alterations in myocardium in relation to changing optical-properties," *Appl. Opt.* **32**(4), 461–463 (1993).
23. S. Thomsen, S. L. Jacques, and S. Flock, "Microscopic correlates of optical property changes during thermal coagulation of myocardium," *Proc. SPIE* **1202**, 2–11 (1990).
24. J. R. Mourant, I. J. Bigio, D. A. Jack, T. M. Johnson, and H. D. Miller, "Mechanisms of light scattering from biological cells relevant to noninvasive optical-tissue diagnostics," *Appl. Opt.* **37**(16), 3586–3593 (1998).
25. M. Pop, A. Molckovsky, L. Chin, M. C. Kolios, M. A. S. Jewett, and M. Sherar, "Changes in dielectric properties at 460 kHz of kidney and fat during heating: importance for radio-frequency thermal therapy," *Phys. Med. Biol.* **48**(15), 2509–2525 (2003).
26. R. Schober, F. Ulrich, T. Sander, H. Durselen, and S. Hessel, "Laser-induced alteration of collagen substructure allows microsurgical tissue welding," *Science* **232**(4756), 1421–1422 (1986).
27. J. Tang, G. Godlewski, S. Rouy, and G. Delacretaz, "Morphologic changes in collagen fibers after 830 nm diode laser welding," *Lasers Surg. Med.* **21**(5), 438–443 (1997).